SANDIA REPORT
SAND2009-5705
Unlimited Release
Printed September 2009

Computational Investigation of Thermal Gas Separation for CO_2 Capture

John R. Torczynski, Michael A. Gallis, Carlton F. Brooks, Patrick V. Brady, and Charles R. Bryan

Prepared by
Sandia National Laboratories
Albuquerque, New Mexico 87185 and Livermore, California 94550

Sandia is a multiprogram laboratory operated by Sandia Corporation,
a Lockheed Martin Company, for the United States Department of Energy's
National Nuclear Security Administration under Contract DE-AC04-94AL85000.

Issued by Sandia National Laboratories, operated for the United States Department of Energy by Sandia Corporation.

Available to DOE and DOE contractors from
U.S. Department of Energy
Office of Scientific and Technical Information
P.O. Box 62
Oak Ridge, TN 37831

Telephone: (865) 576-8401
Facsimile: (865) 576-5728
E-Mail: reports@adonis.osti.gov
Online ordering: http://www.osti.gov/bridge

Available to the public from
U.S. Department of Commerce
National Technical Information Service
5285 Port Royal Rd.
Springfield, VA 22161

Telephone: (800) 553-6847
Facsimile: (703) 605-6900
E-Mail: orders@ntis.fedworld.gov
Online order: http://www.ntis.gov/help/ordermethods.asp?loc=7-4-0#online

SAND2009-5705
Unlimited Release
Printed September 2009

Computational Investigation of Thermal Gas Separation for CO_2 Capture

John R. Torczynski, Michael A. Gallis, and Carlton F. Brooks
Microscale Science and Technology Department
Sandia National Laboratories
P.O. Box 5800
Albuquerque, New Mexico 87185-0346

Patrick V. Brady
Geoscience Research and Applications Group
Sandia National Laboratories
P.O. Box 5800
Albuquerque, New Mexico 87185-0754

Charles R. Bryan
Yucca Mountain Project Upper Barrier System Department
Sandia National Laboratories
P.O. Box 5800
Albuquerque, New Mexico 87185-0776

Abstract

This report summarizes the work completed under the Laboratory Directed Research and Development (LDRD) project 09-1351, "Computational Investigation of Thermal Gas Separation for CO_2 Capture". Thermal gas separation for a binary mixture of carbon dioxide and nitrogen is investigated using the Direct Simulation Monte Carlo (DSMC) method of molecular gas dynamics. Molecular models for nitrogen and carbon dioxide are developed, implemented, compared to theoretical results, and compared to several experimental thermophysical properties. The molecular models include three translational modes, two fully excited rotational modes, and vibrational modes, whose degree of excitation depends on the temperature. Nitrogen has one vibrational mode, and carbon dioxide has four vibrational modes (two of which are degenerate). These models are used to perform a parameter study for mixtures of carbon dioxide and nitrogen confined between parallel walls over realistic ranges of gas temperatures and nominal concentrations of carbon dioxide. The degree of thermal separation predicted by DSMC is slightly higher than experimental values and is sensitive to the details of the molecular models.

ACKNOWLEDGMENTS

This work was performed at Sandia National Laboratories. Sandia is a multiprogram laboratory operated by Sandia Corporation, a Lockheed Martin Company, for the United States Department of Energy's National Nuclear Security Administration under Contract DE-AC04-94AL85000. The authors wish to express their appreciation to the Laboratory Directed Research and Development (LDRD) office at Sandia National Laboratories and the U.S. Department of Energy (DOE) for funding this project, denoted LDRD 09-1351. The authors thank Ellen B. Stechel and Daniel J. Rader of Sandia National Laboratories for many helpful discussions.

TABLE OF CONTENTS

LIST OF FIGURES

LIST OF TABLES

NOMENCLATURE

Variables

C_p	specific heat at constant pressure (J/kg·K)
C_v	specific heat at constant volume (J/kg·K)
D	mass diffusivity (m^2/s)
e	thermal energy per unit mass (J/kg)
K	thermal conductivity (W/m·K)
k_B	Boltzmann constant (J/K)
m	molecular mass (kg)
n	number density ($1/m^3$)
n_{i0}	concentration (number fraction) of component i (1)
p	pressure (Pa)
q	heat flux (W/m^2)
R	ideal gas constant (J/kg·K)
T	temperature (K)
$\mathbf{u}$	velocity vector (m/s)
u, v, w	Cartesian components of velocity (m/s)
$\mathbf{x}$	position vector (m)
x, y, z	Cartesian components of position (m)
Z	collision number (1)

Greek Variables

α	VSS angular scattering exponent (1)
α_{12}	thermal diffusion factor for a binary gas mixture (1)
β	mass conductivity (kg/m·s)
μ	absolute shear viscosity (Pa·s)
ρ	mass density (kg/m^3)
τ	shear stress (Pa)
Θ	temperature scale for an internal energy mode (K)
ω	VSS viscosity temperature exponent (1)

Subscripts

$(\cdots)_1$	component 1 (heavier)
$(\cdots)_2$	component 2 (lighter)
$(\cdots)_{\text{ref}}$	reference
$(\cdots)_{\text{rot}}$	rotational
$(\cdots)_{\text{vib}}$	vibrational

Acronyms

DSMC	Direct Simulation Monte Carlo
HO	Harmonic Oscillator
LB	Larsen-Borgnakke
LDRD	Laboratory Directed Research and Development
VSS	Variable Soft Sphere

1. INTRODUCTION

1.1. Deliverable

This report summarizes the work completed for the Laboratory Directed Research and Development (LDRD) project 09-1351, "Computational Investigation of Thermal Gas Separation for CO_2 Capture". The project's goal is to quantify thermal gas separation of carbon dioxide from nitrogen, the main component of air. Three steps are involved in this process.

1. Implement and assess molecular models for nitrogen and carbon dioxide.
2. Perform a parameter study over a wide range of temperatures.
3. Perform a parameter study over a wide range of nominal carbon dioxide concentrations.

1.2. Approach

The Direct Simulation Monte Carlo (DSMC) method of molecular gas dynamics (Bird, 1994) is used to simulate mixtures of nitrogen and carbon dioxide. Although DSMC is not limited to binary gas mixtures, a two-component mixture can be investigated without the additional complexity encountered in multi-component mixtures (Bird, Stewart, and Lightfoot, 1960, 2007; Hirschfelder, Curtiss, and Bird, 1954). Nitrogen is used for the carrier gas because it is the dominant component of air and has thermophysical properties similar to those of air (White, 1984). All DSMC simulations reported herein are performed with Sandia's one-dimensional massively parallel DSMC code DSMC1, which employs the same basic algorithm used in Sandia's two-dimensional massively parallel DSMC code Icarus (Bartel et al., 2001).

Molecular models for nitrogen and carbon dioxide are developed, implemented, and assessed by comparison to experimentally measured thermophysical properties. These models include three translational modes, two fully excited rotational modes (appropriate for linear molecules), and vibrational modes, whose degree of excitation depends on temperature. Nitrogen has one vibrational mode, and carbon dioxide has four vibrational modes (two are degenerate). These models are assessed by comparison to theoretical results and to experimentally measured thermophysical properties: the specific heat at constant pressure, the thermal conductivity, the viscosity, and the mass conductivity (the product of mass density and mass diffusivity). This comparison is performed over a wider temperature range (300-1200 K) than is expected to be encountered in thermal gas separation.

DSMC is subsequently used to perform a parameter study of thermal diffusion of carbon dioxide in nitrogen for wide ranges of nominal temperatures and nominal concentrations of carbon dioxide. The computed temperature and concentration profiles are used to determine the corresponding thermal separation factors, which are compared to experimental measurements, where available. The degree of agreement suggests that DSMC can be used to study thermal diffusion in gas mixtures with reasonable accuracy if sufficiently accurate molecular models for carbon dioxide and nitrogen are available over the temperature range of interest.

2. THERMAL GAS SEPARATION

2.1. Overview

The process of thermal diffusion in gases, the physical principle underlying thermal gas separation, is described. The enhancement of thermal gas separation that can be achieved in a Clusius-Dickel column from thermally-driven buoyant convection is illustrated.

2.2. Physical Process

Thermal diffusion occurs in nonisothermal gas mixtures. More specifically, lighter components are preferentially concentrated in the hotter regions, and heavier components are preferentially concentrated in the colder regions (Clark Jones and Furry, 1946; Grew and Ibbs, 1952; Hirschfelder, Curtiss, and Bird, 1954; Bird, Stewart, and Lightfoot, 1960, 2007; Chapman and Cowling, 1970). Consider a binary gas mixture at pressure p and temperature T with the heavier and lighter components, denoted by "1" and "2", having number densities n_1 and n_2, total number density $n = n_1 + n_2$, and concentrations $n_{10} = n_1/n$ and $n_{20} = n_2/n$ so that $n_{10} + n_{20} = 1$. When temperature or concentration gradients are present, the mean velocities $\mathbf{u}_1$ and $\mathbf{u}_2$ differ (Grew and Ibbs, 1952) according to the following three equivalent expressions, where D_{12} is the concentration diffusion coefficient, D_T is the thermal diffusion coefficient, $k_T = D_T/D_{12}$ is the thermal diffusion ratio, and $\alpha_{12} = k_T/n_{10}n_{20}$ is the thermal diffusion factor:

$$\begin{aligned}
\mathbf{u}_1 - \mathbf{u}_2 &= -\frac{1}{n_{10}n_{20}}\left\{D_{12}\frac{\partial n_{10}}{\partial \mathbf{x}} + D_T\frac{1}{T}\frac{\partial T}{\partial \mathbf{x}}\right\},\\
\mathbf{u}_1 - \mathbf{u}_2 &= -\frac{D_{12}}{n_{10}n_{20}}\left\{\frac{\partial n_{10}}{\partial \mathbf{x}} + k_T\frac{1}{T}\frac{\partial T}{\partial \mathbf{x}}\right\},\\
\mathbf{u}_1 - \mathbf{u}_2 &= -\frac{D_{12}}{n_{10}n_{20}}\left\{\frac{\partial n_{10}}{\partial \mathbf{x}} + \alpha_{12}n_{10}n_{20}\frac{1}{T}\frac{\partial T}{\partial \mathbf{x}}\right\}.
\end{aligned} \tag{1}$$

The thermal diffusion factor α_{12} has the following properties (Grew and Ibbs, 1952). It is relatively insensitive to the concentration values. It increases as the ratio m_1/m_2 of the heavier to the lighter molecular masses increases. It is largest when the molecular interactions are elastic hard sphere. Grew and Ibbs (1952) provide tables with values of α_{12} for different mixtures and different temperatures, with all reported values lying in the range $-0.010 \le \alpha_{12} \le 0.64$. Some values have substantial uncertainty. For example, the values for nitrogen and carbon dioxide around 300 K lie in the range $0.036 \le \alpha_{12} \le 0.061$.

Equation (1) indicates that a quiescent gas mixture with a steady temperature gradient also has concentration gradients. Based on the signs of the terms in this equation and the fact that α_{12} is almost always positive, component 1 (the heavier component) is preferentially concentrated in the colder regions, and component 2 (the lighter component) is preferentially concentrated in the hotter regions, as asserted earlier. Figure 2.1 qualitatively illustrates thermal separation for a quiescent binary gas mixture confined between motionless isothermal parallel walls and the effect of flow on the distribution of the two components.

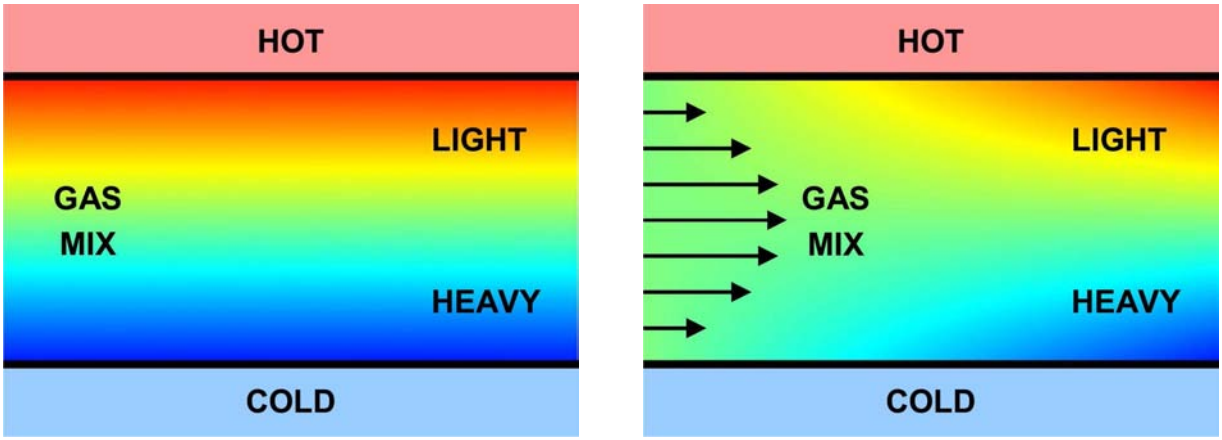

Figure 2.1. Thermal gas separation: left, stationary gas; right, flowing gas.

When the concentration variations are small compared to their nominal values and when the thermal diffusion factor α_{12} is independent of temperature, Equation (1) can be integrated from one wall to the other to determine the concentration difference thus obtained:

$$\Delta n_{10} = n_{10}^{\text{cold}} - n_{10}^{\text{hot}} = n_{20}^{\text{hot}} - n_{20}^{\text{cold}} = \alpha_{12} n_{10} n_{20} \ln\left[\frac{T^{\text{hot}}}{T^{\text{cold}}}\right], \quad \Delta n_{10} << n_{10}. \tag{2}$$

For example, with a thermal diffusion factor of approximately 0.05, a 50/50 mixture of nitrogen and carbon dioxide (i.e., both concentrations are 0.50) confined between walls with temperatures of 300 K and 600 K has a concentration difference of $\Delta n_{10} = 0.0087$ (less than 1%) and a relative concentration difference of $\Delta n_{10}/n_{10} = 0.017$ from one wall to another.

When the heavier component is a trace constituent (i.e., its concentration is very small), Equation (2) can be simplified:

$$\frac{\Delta n_{10}}{n_{10}} = \alpha_{12} \ln\left[\frac{T^{\text{hot}}}{T^{\text{cold}}}\right], \quad \Delta n_{10} << n_{10} << 1. \tag{3}$$

For the above example, the relative concentration difference in this limit is $\Delta n_{10}/n_{10} = 0.035$ (i.e., twice that for the 50/50 mixture).

As this example indicates, it is difficult to achieve large concentration differences (either absolute or relative) because of the smallness of the thermal diffusion factor and the logarithmic dependence on temperature. This observation points out the need for a flow-based method that can enhance thermal separation substantially above these quiescent-gas values.

2.3. Column Implementation

A Clusius-Dickel column uses buoyancy-driven convection to establish a counter-current flow that can substantially enhance thermal separation (Clark Jones and Furry, 1946; Grew and Ibbs, 1952; Hirschfelder, Curtiss, and Bird, 1954; Bird, Stewart, and Lightfoot, 1960, 2007). Their original experiments use a vertical tube cooled by water flowing down its exterior and heated within by a current-carrying wire along the axis. Diameters are typically around 1 cm, and heights are typically around 1 m. The radial temperature gradient produced by the electrically-heated wire and the water-cooled wall has two effects. First, this temperature gradient induces a buoyancy-driven convection flow that is upward along the axis and downward along the wall. Second, this temperature gradient induces a radial concentration gradient, with the lighter component concentrated near the axis and the heavier component concentrated near the wall. The conveyor-belt nature of the counter-current buoyancy-driven convection flow acts to transport the lighter component to the top of the column and the heavier component to the bottom of the column. In this manner, substantially larger concentration differences can be achieved than can be achieved using temperature gradients in quiescent gas.

Figure 2.2 schematically indicates how buoyant convection enhances thermal separation. Consider a vertical geometry bounded by a cold wall on the left and a hot wall on the right, and partition this geometry into square cells, with the gap spanned by two cells. Fill all cells with a binary gas mixture in which each component has an initial concentration of 50%. Assume that thermal diffusion produces a lateral concentration difference of 4% independent of the gas composition. Buoyant convection causes the gas to be transported upward on the right side, leftward at the top, downward on the left side, and rightward on the bottom. Apply alternating steps of thermal diffusion and buoyant convection as above, and average the cell values from these two steps. After each successive pair of thermal-diffusion and buoyant-convection steps, the vertical concentration variation seen in their average becomes larger, with the ultimate limit shown in the lower right of the figure. In this highly simplified example, thermal diffusion alone can produce only a 4% difference (i.e., 52% vs. 48%), whereas thermal diffusion and buoyant convection operating together can produce a 28% difference (i.e., 64% vs. 36%) from bottom to top, which is a 7-fold improvement. In this example, the separation that ultimately can be achieved is determined by the values assumed for lateral thermal separation (i.e., 52% vs. 48%) and the number of cells in the vertical direction (i.e., 8). In principle, an infinite number of cells in the vertical direction would lead to complete separation at the bottom and top of the column (i.e., 100% vs. 0%, rather than 64% vs. 36%) even when the mass ratio is near unity, as for isotopes. However, infinite time is required to achieve these values.

Although Clusius-Dickel columns generally use the wire-tube geometry discussed above, the Clusius-Dickel approach can also be implemented in a slot geometry with two parallel walls, one of which is hot and the other of which is cold. Clusius-Dickel columns can be combined in a series-parallel fashion to achieve even larger concentration differences (Grew and Ibbs, 1952). Maintaining steady laminar buoyant-convection flow limits the size of a Clusius-Dickel column (Grew and Ibbs, 1952). A Clusius-Dickel column can be used to join two large reservoirs, but the time to achieve steady concentration differences may become long (Grew and Ibbs, 1952).

Thermal gas separation thus has two aspects. The first is the degree of lateral separation that can be achieved, which is the focus of this report. The second is enhancement through counter-flow from buoyant convection or through other flow-based approaches.

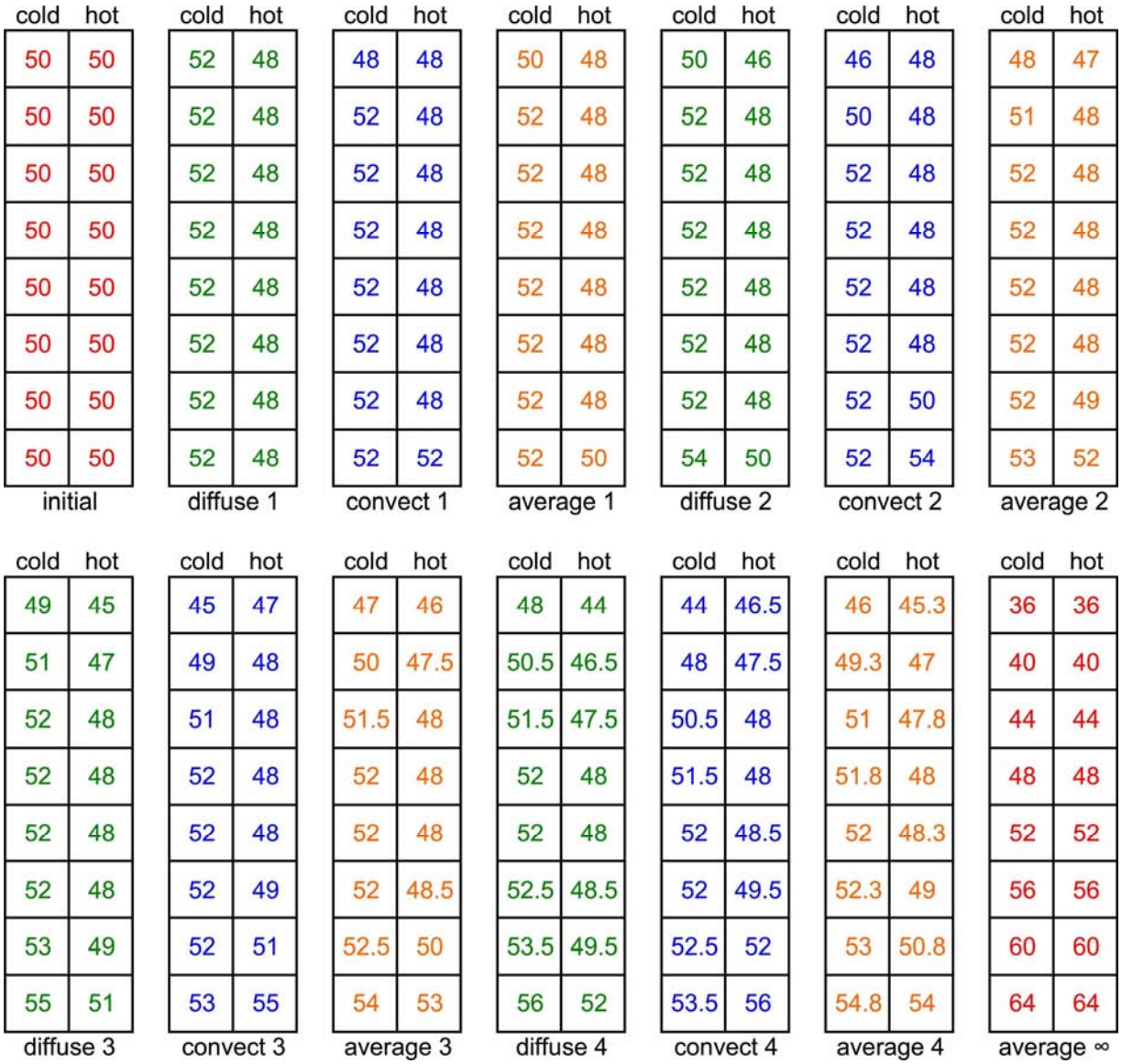

Figure 2.2. Schematic diagram of thermal gas separation in a Clusius-Dickel column.

3. DIRECT SIMULATION MONTE CARLO SIMULATIONS

3.1. Overview

The Direct Simulation Monte Carlo (DSMC) method of molecular gas dynamics is briefly discussed. Molecular models for the internal energy and collision dynamics of nitrogen and carbon dioxide are presented. The thermophysical properties from DSMC simulations using these models are compared to experimental values. DSMC simulations are performed for mixtures of nitrogen and carbon dioxide with 7 nominal concentrations and 4 mean temperatures. The thermal diffusion factor is determined for each of these 28 cases, and this set of values is compared to experimental values. The DSMC results are shown to be sensitive to the molecular model for carbon dioxide.

3.2. Description of Computational Method

The Direct Simulation Monte Carlo (DSMC) method of molecular gas dynamics (Bird, 1994; Bartel et al., 2001) is illustrated schematically in Figure 3.1. DSMC uses computational molecules, termed "simulators", to represent a gas. Typically, each simulator represents a large number of real gas molecules. Gas mixtures are treated straightforwardly by having one type of simulator for each component in the mixture. During a time step, simulators move ballistically at their velocities, reflect from walls (specularly, diffusely, or any combination thereof), and collide in a pairwise fashion. Collisions occur at the expected rate and conserve mass, momentum, and energy. The post-collision states of the simulators reproduce the statistics of collisions between real molecules. Macroscopic gas properties are obtained by sampling the properties of the simulators within each cell. For a steady situation, these properties can be averaged over long times to reduce statistical uncertainty (the ergodic hypothesis).

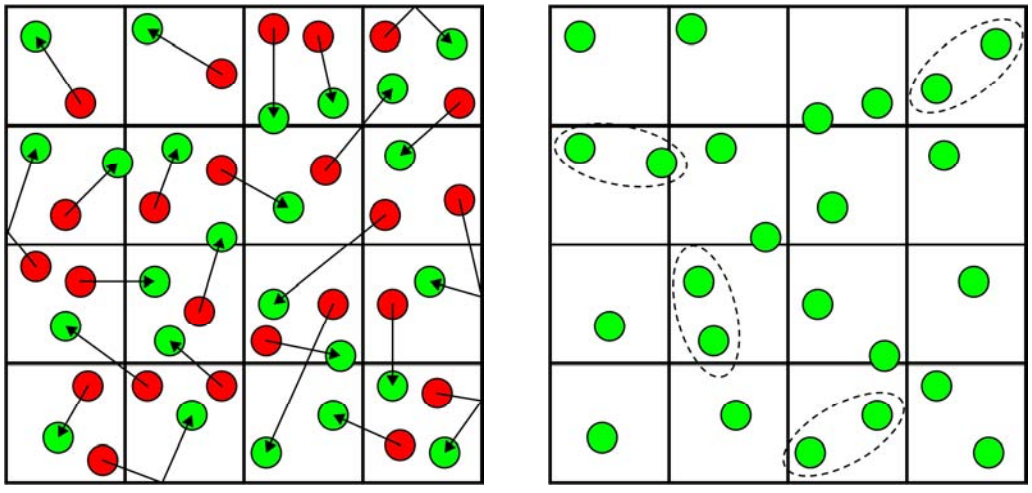

Figure 3.1. DSMC algorithm steps: left, molecular motion; right, molecular collision.

3.3. Molecular Models

For each component in a gas mixture, molecular models are needed that describe its internal energy (rotational and vibrational) and its collision dynamics.

Figure 3.2 and Figure 3.3 illustrate the energy modes of nitrogen and carbon dioxide, respectively. Both molecules have 3 translational modes, which correspond to motions in the 3 Cartesian directions, and, being linear molecules, 2 rotational modes, which correspond to rotations about the two orthogonal axes with appreciable moments of inertia (i.e., not the axis along the linear direction of the molecule). Nitrogen and carbon dioxide have vibrational modes, with each mode having both potential and kinetic energy. Nitrogen has 1 vibrational mode, corresponding to oppositely moving nitrogen atoms. Carbon dioxide has 4 vibrational modes: 2 equivalent bending modes, in which the oxygen atoms move oppositely to the carbon atom, and 2 distinct stretching modes, in which all atoms move collinearly as indicated in the figure.

The Harmonic Oscillator (HO) model is used to describe the vibrational energy modes of these molecules (Bird, 1994). Each vibrational mode i is characterized by a vibrational temperature $\Theta_{\text{vib},i}$ that describes the spacing between the energy levels of that mode, $k_B\Theta_{\text{vib},i}$, where k_B is the Boltzmann constant. For a linear molecule (i.e., with 2 rotational energy modes) with mass m and ideal gas constant $R = k_B/m$, the specific heat at constant volume, C_v, and the specific heat at constant pressure, C_p, have the following forms:

$$\frac{C_p}{R} = \frac{C_v}{R} + 1 = \frac{7}{2} + \sum_i \left(\frac{\Theta_{\text{vib},i}/2T}{\sinh\left[\Theta_{\text{vib},i}/2T\right]} \right)^2 . \tag{4}$$

For temperatures that are small compared to all vibrational temperatures, the summands vanish, yielding the known specific heats for linear molecules without vibration. For temperatures that are large compared to all vibrational temperatures, the summands all approach unity, yielding 2 units of $k_BT/2$ for each vibrational energy mode (i.e., potential and kinetic energy).

The DSMC simulations described herein all use the Variable Soft Sphere (VSS) model to describe molecular collisions and the Larsen-Borgnakke (LB) model to describe internal energy exchange during collisions (Bird, 1994; Bartel et al., 2001). In brief, the VSS model describes each type of simulator in terms of a reference viscosity μ_{ref} at a reference temperature T_{ref}, a viscosity temperature exponent ω, and an angular scattering exponent α (Bird, 1994). For the VSS model, the viscosity μ, the temperature T, the mass density ρ, the self-diffusion coefficient D, and the mass self-conductivity β obey the below expressions (Bird, 1994):

$$\frac{\mu}{\mu_{\text{ref}}} = \left(\frac{T}{T_{\text{ref}}} \right)^{\omega}, \quad \frac{\beta}{\mu} = \frac{\rho D}{\mu} = \frac{3(7-2\omega)\alpha}{5(2+\alpha)} . \tag{5}$$

Thus, in the VSS model, the mass conductivity (i.e., the product of mass density and diffusivity) is always exactly proportional to the viscosity. The detailed collision statistics for each molecule is determined by the above VSS parameters (Bird, 1994). The parameters μ_{ref}, T_{ref}, ω, and α are usually determined by fitting the experimentally measured viscosity and diffusivity over a prescribed temperature range. Bird (1994) provides a table of values for many common gases.

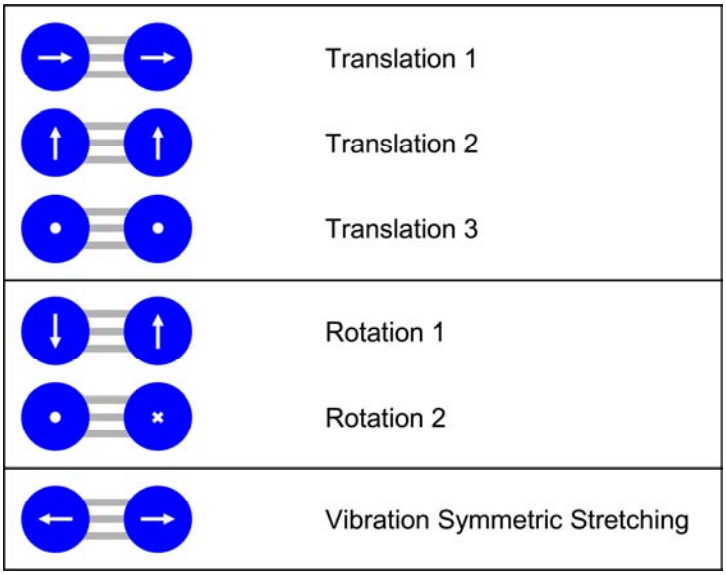

Figure 3.2. Energy modes of a nitrogen molecule.

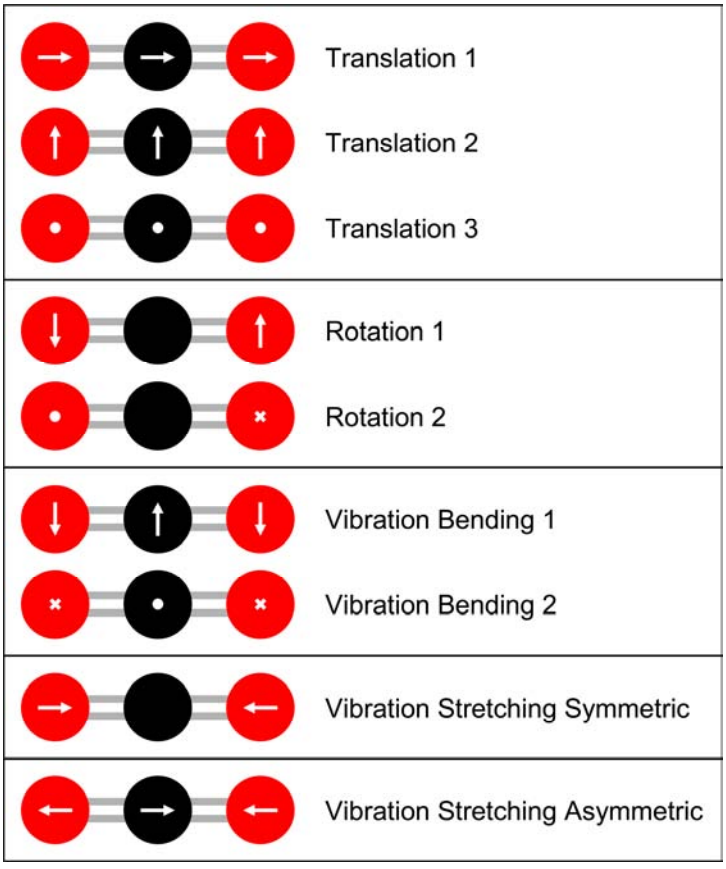

Figure 3.3. Energy modes of a carbon dioxide molecule.

Bird, Stewart, and Lightfoot (1960, 2007) provide an estimate of the thermal conductivity K for a pure gas. However, this estimate is independent of the rotational and vibrational collision numbers Z_{rot} and Z_{vib}, discussed below, which can affect the thermal conductivity. The following expression uses the thermophysical form of this estimate scaled by a reference value K_{ref} at T_{ref} to estimate the thermal conductivity of a VSS gas:

$$\frac{K}{K_{\text{ref}}} = \frac{\mu}{\mu_{\text{ref}}} \frac{C_v}{C_{v,\text{ref}}}. \tag{6}$$

When a collision occurs in a DSMC simulation, internal energy may be exchanged with translational energy. If a particular internal energy mode exchanges energy with the translational modes, the LB model governs this exchange (Bird, 1994). The probabilities that rotational and vibrational energy are exchanged are essentially the inverses of the rotational and vibrational collision numbers, Z_{rot} and Z_{vib}, respectively. For example, values of $Z_{\text{rot}} = 5$ and $Z_{\text{vib}} = 10^8$ mean that a simulator will exchange rotational energy during 1 out of every 5 collisions on average and vibrational energy during 1 out of every 10^8 collisions on average. The limiting values of Z_{rot} and Z_{vib} are 1 (maximum energy exchange) and ∞ (zero energy exchange).

Both components require molecular models for Z_{rot} and Z_{vib}. Bird (1994) suggests the following models for nitrogen over a wide temperature range:

$$Z_{\text{rot}} = \frac{Z_{\text{rot}}^{\infty}}{1 + \left(\pi^{3/2}/2\right)\left(T^*/T\right)^{1/2} + \left(\pi + \pi^2/4\right)\left(T^*/T\right)}, \; Z_{\text{rot}}^{\infty} = 15.7, \; T^* = 80.0 \text{ K};$$

$$Z_{\text{vib}} = C_1 \left(T/T^+\right)^{-\omega} \exp\left[C_2 \left(T/T^+\right)^{-1/3}\right], \; C_1 = 9.1, \; C_2 = 220.0, \; T^+ = 1 \text{ K}. \tag{7}$$

However, these models rely on the macroscopic temperature, which is contrary to the general tenet of DSMC that only molecular-level quantities should be used for determining collisions. Moreover, accurate molecular models for carbon dioxide have not yet been developed, in part because a Z_{vib} model is needed for each of the 3 non-degenerate vibrational energy modes. In the absence of molecular-level Z_{rot} and Z_{vib} models for nitrogen and carbon dioxide, constant values are used. Additionally, the same value is used for all four vibrational modes of carbon dioxide. The nitrogen values are selected to be in accord with values from the above models of Bird (1994), and the carbon dioxide values are selected to be those suggested by Lambert (1977).

Table 3.1 contains all molecular properties used in the DSMC simulations. Most of these values are taken from Bird (1994). Notable exceptions are the ω and α values for carbon dioxide. The values of Bird, included in parentheses, are replaced by values that approximately represent the viscosity over 300-600 K rather than representing the viscosity very accurately over a narrow temperature range around 300 K. Both sets of values have the same ratio of the mass conductivity to the viscosity, as in Equation (5).

Table 3.1. Molecular properties of nitrogen and carbon dioxide for DSMC simulations.

Property	Symbol	Nitrogen	Carbon Dioxide
Boltzmann constant	k_B	1.380658×10^{-23} J/K	1.380658×10^{-23} J/K
Molecular mass	m	46.5×10^{-27} kg	73.1×10^{-27} kg
Reference temperature	T_{ref}	273.15 K	273.15 K
Reference viscosity	μ_{ref}	1.656×10^{-5} Pa·s	1.380×10^{-5} Pa·s
Reference thermal conductivity	K_{ref}	0.0240 W/m·K	0.0146 W/m·K
Viscosity temperature exponent	ω	0.74	0.86 (Bird: 0.93)
Angular scattering exponent	α	1.36	1.54 (Bird: 1.61)
Rotational collision number	Z_{rot}	5.0	2.5
Vibrational collision number	Z_{vib}	10^{20}	5.3
Vibrational temperature(s)	Θ_{vib}	3374.2 K	945 K (2)
			1903 K (1)
			3339 K (1)

3.4. Thermophysical-Property Simulations

DSMC simulations are performed to assess the ability of the models discussed in the previous section to reproduce the experimentally measured thermophysical properties of nitrogen and carbon dioxide. In particular, the specific heat at constant pressure, the thermal conductivity, the viscosity, and the mass conductivity should be accurately represented over the requisite temperature range. Figure 3.4 shows the two flows used to determine these properties. In Fourier flow, the gas is confined between two parallel motionless walls with unequal temperatures and unity accommodation (probability that an incident gas molecule exchanges energy with the wall on reflection). At steady state, the heat flux q is uniform throughout the domain, and the temperature profile is approximately linear, with small discontinuities at the walls caused by the small but finite mean free path. Since the heat flux and the temperature gradient are known, the thermal conductivity is determined from Fourier's Law: $q = -K\,dT/dx$. Similarly, since the thermal energy e per unit mass and the temperature are known, the specific heats at constant pressure and at constant volume are determined from their definitions: $C_p = C_v + R$, $C_v = de/dT$. In Couette flow, the gas is confined between two parallel isothermal walls with opposite tangential velocities and unity accommodation. At steady state, the shear stress τ is uniform throughout the domain, and the profile of the tangential velocity component v is approximately linear, with small discontinuities at the walls caused by the small but finite mean free path. Since the shear stress and the velocity gradient are known, the viscosity is determined from Newton's Law: $\tau = \mu\,dv/dx$. As discussed in the previous section, the mass conductivity β is proportional to the viscosity μ for the VSS molecular model. Figure 3.5 shows typical temperature and tangential-velocity profiles obtained from such DSMC simulations.

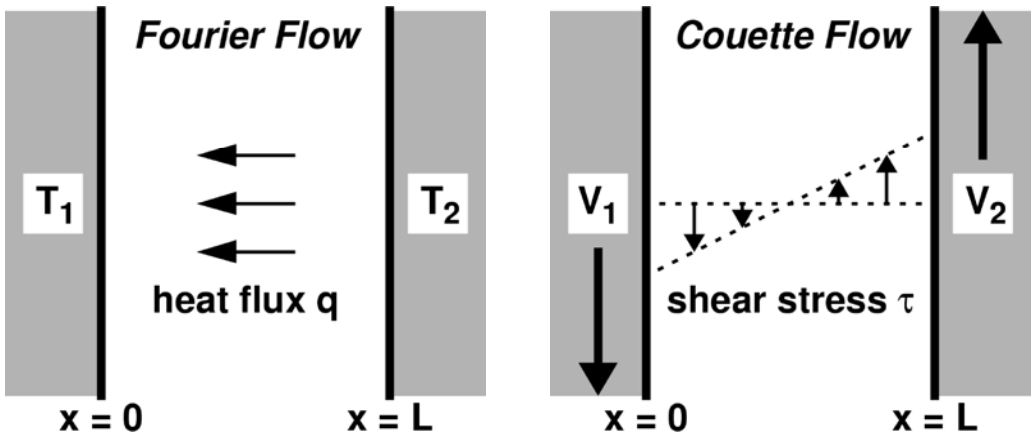

Figure 3.4. Flows for determining thermophysical properties.

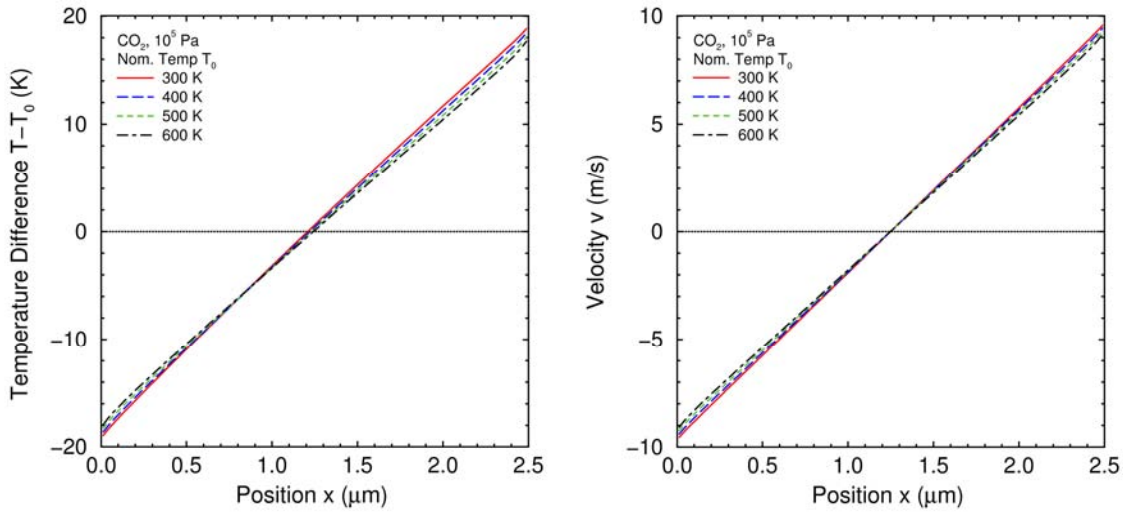

Figure 3.5. Typical profiles for determining thermophysical properties.

All DSMC simulations herein use the following parameters. The gas pressure is 10^5 Pa, and the nominal gas temperature is 300, 600, 900, or 1200 K, with other values for some cases. For Fourier flow, the walls differ by ±25 K from nominal. For Couette flow, the walls move tangentially at ±10 m/s. The domain is 2.5 μm wide and is spanned by 200 cells, each of which initially contains a total of 120 simulators apportioned according to the nominal gas composition. A fixed time step of 10 ps is used. Once steady state is reached, long-time averaging is used to reduce the statistical uncertainty.

Figure 3.6 shows values computed for the specific heat at constant pressure, the thermal conductivity, the viscosity, and the mass conductivity of nitrogen determined by this approach, and Figure 3.7 shows analogous values for carbon dioxide. The red points are experimental values tabulated by White (1984), the green curves are smooth fits through these points to guide the eye, the dashed black curves are the VSS theoretical results in the previous section, the blue circles are the DSMC values using the parameters in Table 3.1, and the cyan symbols in some figures are additional DSMC values discussed below. White (1984) does not present values for the mass conductivity; instead, the values of Winn (1950) and Amdur et al. (1952) are shown.

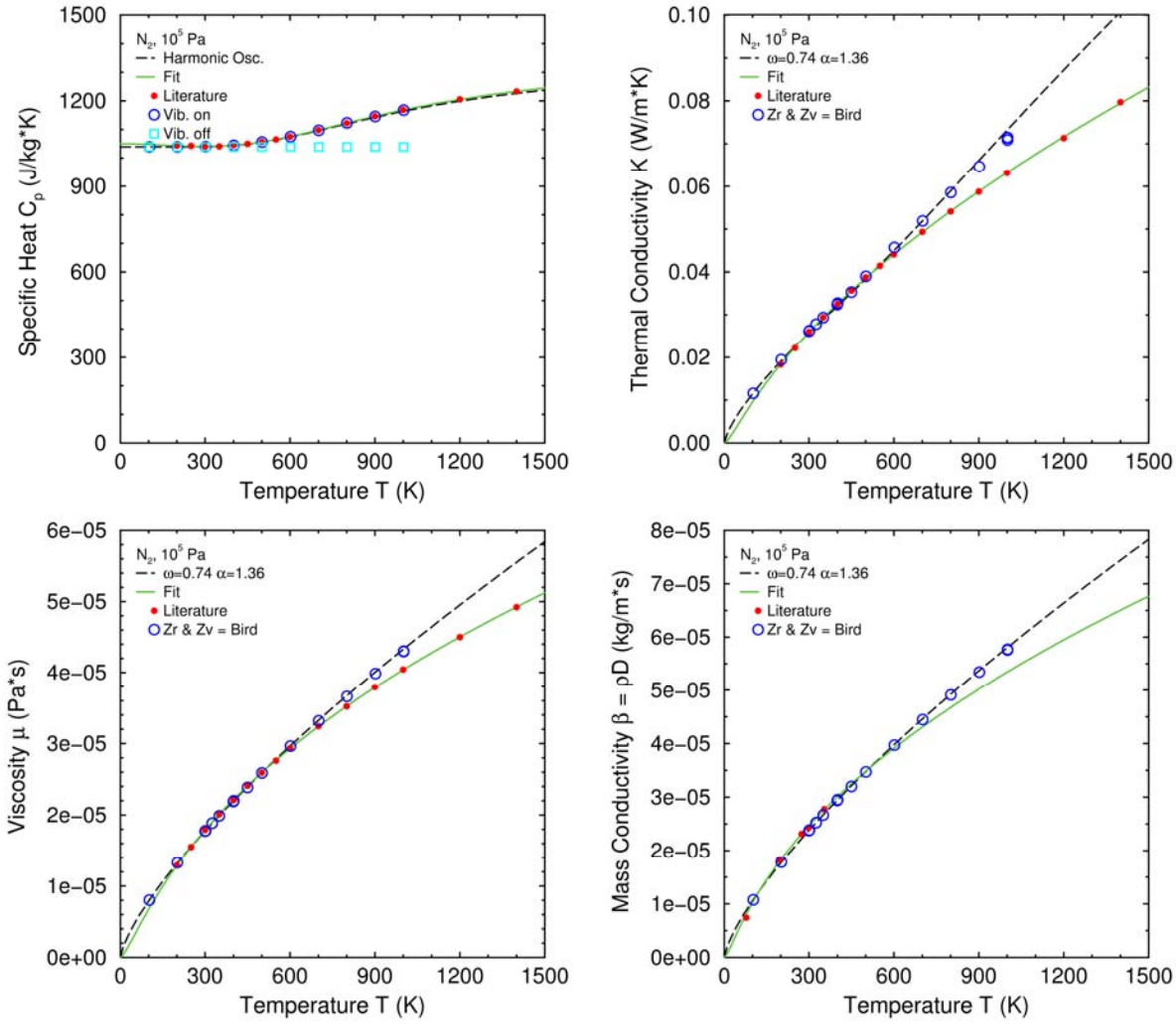

Figure 3.6. Temperature dependence of thermophysical properties of nitrogen.

The nitrogen model described in the previous section represents the experimental thermophysical properties of nitrogen very well in the temperature range of interest, 300-600 K. The specific heat at constant pressure is described by the HO model with excellent accuracy over the entire temperature range, 100-1500 K. The specific heat without any vibrational energy is represented by the square cyan symbols. Vibration is seen to become significant above 600 K. Above 600 K, the theoretical and numerical DSMC values for the thermal conductivity, the viscosity, and the mass conductivity remain in agreement but become progressively larger than the experimental values (there are very few experimental values for the mass conductivity). Thus, the nitrogen models are judged to be good within 300-600 K but only fair above 600 K.

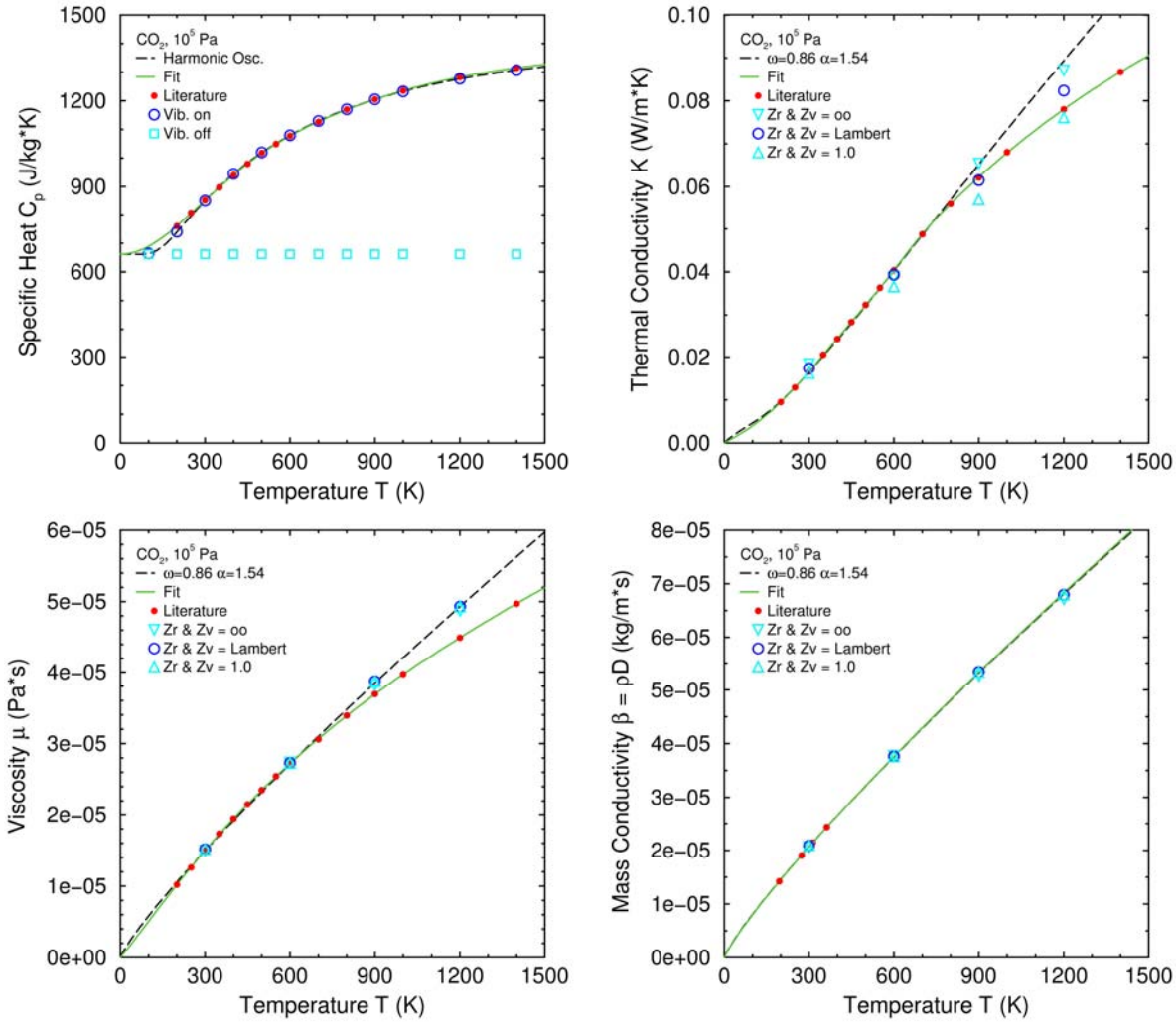

Figure 3.7. Temperature dependence of thermophysical properties of carbon dioxide.

The carbon dioxide model described in the previous section represents the experimental thermophysical properties of carbon dioxide fairly well in the temperature range of interest, 300-600 K. The specific heat at constant pressure is described by the HO model with excellent accuracy over almost the entire temperature range, 100-1500 K. The specific heat without any vibrational energy is represented by the square cyan symbols. Vibration becomes significant above 200 K and dominant above 1400 K. The cyan triangles on the plots for thermal conductivity, viscosity, and mass conductivity represent DSMC simulations performed with the limiting values of Z_{rot} and Z_{vib}, namely ∞ and 1. Above 600 K, the theoretical and numerical DSMC values for the viscosity and the mass conductivity remain in agreement but become progressively larger than the experimental values. Although there are very few experimental values for the mass conductivity, the model is in fair agreement with these values. The thermal conductivity varies considerably with the values of Z_{rot} and Z_{vib}, and limiting values generally bracket the experimental values. The Lambert (1977) values are fairly close to the experimental results although they are sometimes higher and sometimes lower. Thus, the carbon dioxide models are judged to be fair within 300-600 K but only marginal above 600 K.

3.5. Thermal-Diffusion Simulations

DSMC thermal-diffusion simulations are performed for mixtures of nitrogen and carbon dioxide using the Fourier-flow geometry and the DSMC models and parameters of the previous sections. There are 7 nominal carbon dioxide concentrations, namely 0.05, 0.10, 0.20, 0.50, 0.80, 0.90, and 0.95, and 4 nominal gas temperatures (as in the thermophysical-property simulations), namely 300, 600, 900, and 1200 K, yielding a total of 28 combinations. For each of these cases, one value of the thermal diffusion factor α_{12} is computed at the nominal temperature in the following way. At steady state, the average velocity of each component is zero throughout the domain. Equation (1) can be used to represent the thermal diffusion factor α_{12} in terms of the values and gradients of the carbon dioxide concentration n_{10}, the nitrogen concentration $n_{20} = 1 - n_{10}$, and the temperature T:

$$\alpha_{12} = \frac{-T\left(dn_{10}/dx\right)}{n_{10}n_{20}\left(dT/dx\right)}. \tag{8}$$

The ratio of the derivatives in Equation (8) is determined essentially using the chain rule: $\left(dn_{10}/dx\right)/\left(dT/dx\right) = \left(dn_{10}/dT\right)$. The temperature and concentration profiles are combined to represent concentration as a function of temperature. A low-order polynomial is fit through this function. The concentration n_{10} and the slope dn_{10}/dT are found at the nominal temperature. These quantities determine the thermal diffusion factor α_{12} at the nominal temperature.

Figure 3.8 shows the 28 temperature profiles obtained in this manner. Because of the long averaging time used in the simulations, the profiles are very smooth, which facilitates use of the chain rule to determine the thermal diffusion factor. These profiles depend only weakly on the nominal carbon dioxide concentration because they are almost linear and are set primarily by the wall temperatures. Although not shown, the corresponding heat-flux values depend strongly on the nominal carbon dioxide concentration.

Figure 3.9 shows the corresponding 28 profiles of the concentration difference Δn_{10}, which is the carbon dioxide concentration with the nominal value subtracted. Several features are apparent. First, all values are small enough for the residual statistical uncertainty to be seen. Second, the profiles scale approximately with $\Delta T/T$, as seen from the ranges of the y-axes. Third, the profiles scale approximately with the product of the nitrogen and carbon dioxide concentrations, namely $n_{10}n_{20}$, with the 50/50 cases exhibiting the largest values and the mirror-image cases (e.g., 20/80 and 80/20) being nearly the same. If these two scalings were exact, the thermal diffusion factor α_{12} would be independent of temperature and composition.

Figure 3.10 plots the 28 values of the thermal diffusion factor in two fashions: first, as a function of temperature T with nominal carbon dioxide concentration n_{10} as a parameter; second, as a function of nominal carbon dioxide concentration n_{10} with temperature T as a parameter. No strong trends with temperature or nominal concentration are observed. Computing the average and root mean square of all 28 values yields a value of $\alpha_{12} = 0.071 \pm 0.009$. This range of values lies somewhat above the range reported by Grew and Ibbs (1952) for values measured around 300 K: $\alpha_{12} = 0.036$-0.061. Bastick et al. (1939) do suggest that the thermal diffusion factor is larger at elevated temperatures than at room temperature.

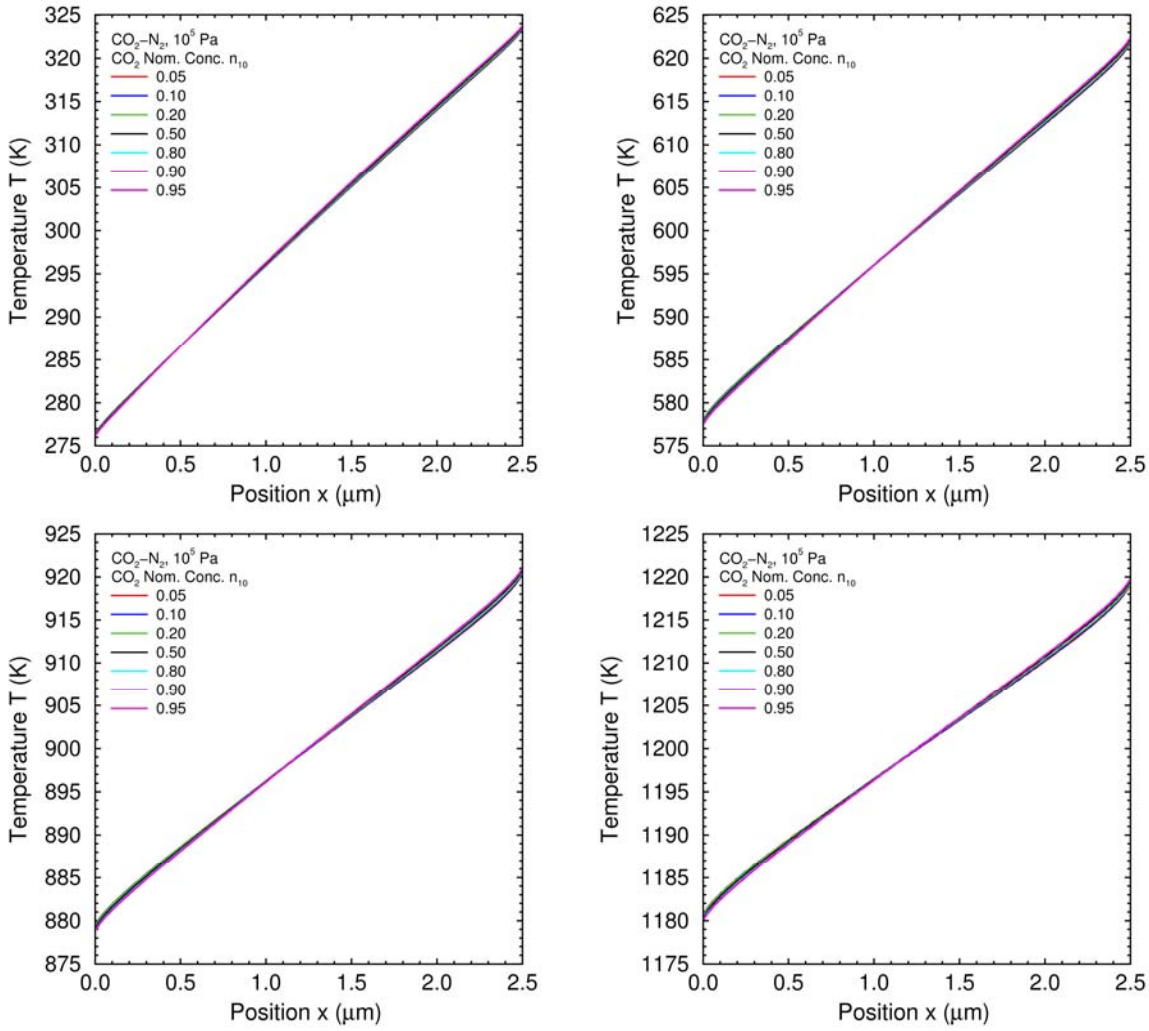

Figure 3.8. Temperature profiles from DSMC thermal-diffusion simulations.

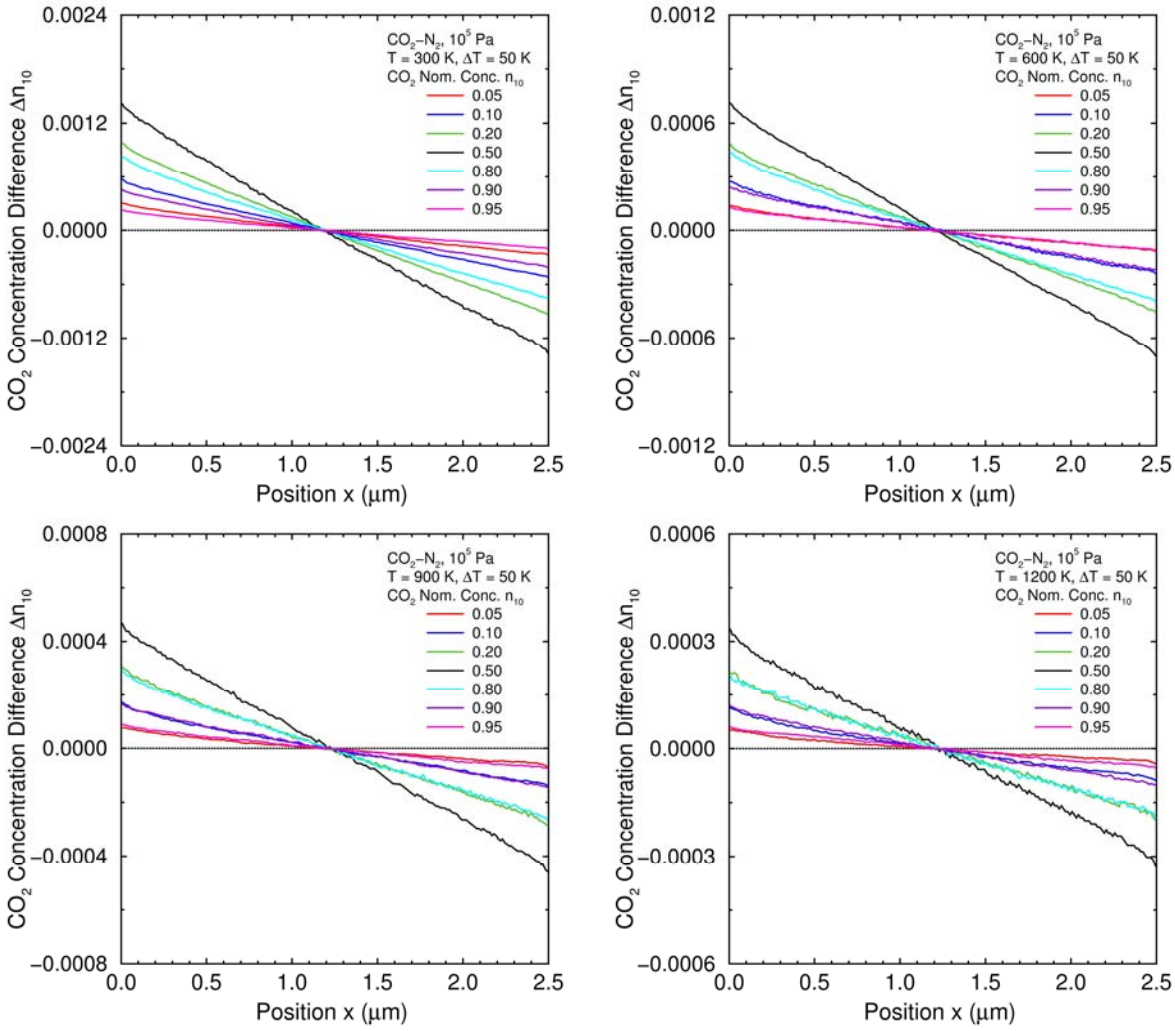

Figure 3.9. CO_2 concentration profiles from DSMC thermal-diffusion simulations.

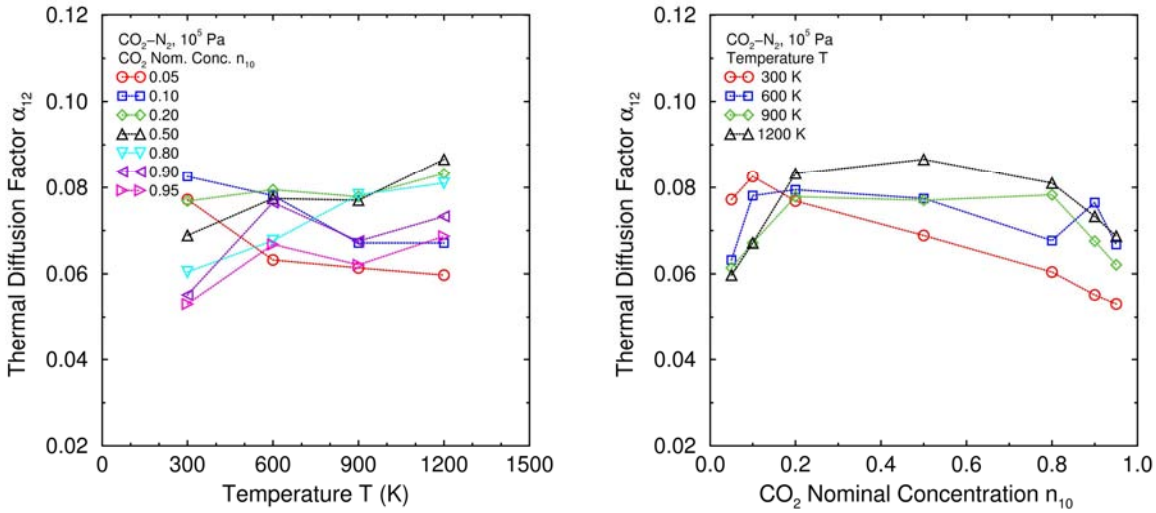

Figure 3.10. Thermal diffusion factor as a function of temperature and CO_2 concentration.

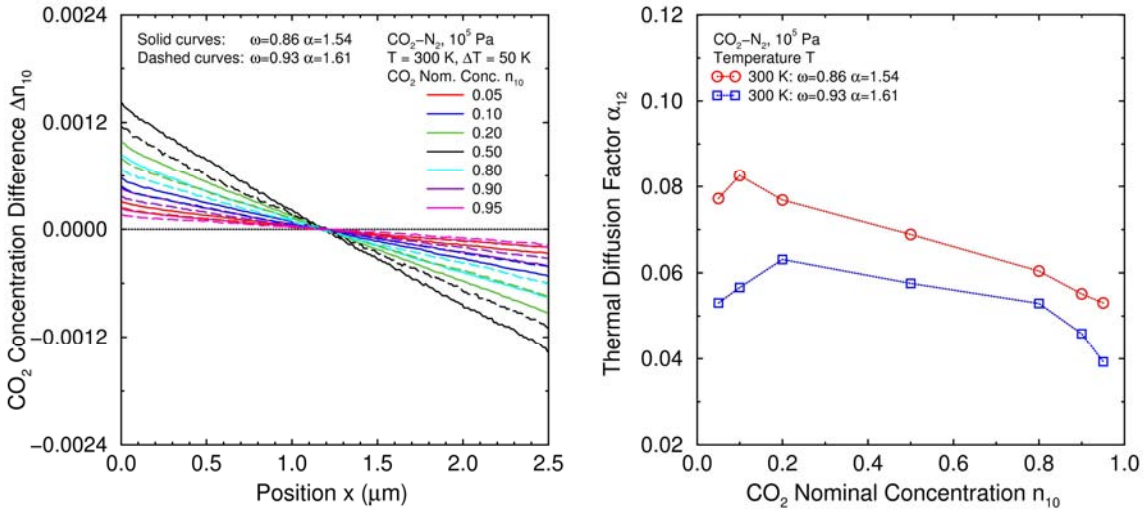

Figure 3.11. Dependence of thermal diffusion at 300 K on carbon dioxide molecular model.

To investigate the dependence of the DSMC results on the carbon dioxide model, additional simulations are performed using the Bird (1994) VSS parameters, shown in Table 3.1. These values match both the viscosity μ and its temperature dependence $d\mu/dT$ at 273.15 K, so simulations are performed for all 7 concentrations but only 1 temperature, 300 K. Figure 3.11 shows the carbon dioxide concentration profiles and the thermal diffusion factors for both sets of VSS parameters. When the Bird (1994) values are used, the concentration profiles and the resulting thermal diffusion factor values are reduced. Although the original values of α_{12} lie within 0.06-0.08, the above Bird (1994) values lie within 0.04-0.06, which is in good agreement with the Grew and Ibbs (1952) values, which lie within 0.036-0.061. While not definitive, this observation suggests that accurate predictions of thermal separation of carbon dioxide from nitrogen require molecular models that represent the viscosity and its temperature dependence accurately over the entire temperature range of interest.

4. CONCLUSIONS

The Direct Simulation Monte Carlo (DSMC) method of molecular gas dynamics is used to simulate thermal separation of carbon dioxide from nitrogen over wide ranges of temperatures and nominal carbon dioxide concentrations. The thermal diffusion factor from all these simulations is found to lie within 0.06-0.08, which is somewhat above the room-temperature experimental values, which lie within 0.036-0.061. The DSMC values are found to be sensitive to the Variable Soft Sphere (VSS) parameters used to describe collisions of carbon dioxide models. Most of the simulations discussed herein use VSS parameters that roughly match the viscosity of carbon dioxide for temperatures in the relevant range of interest, 300-600 K. When VSS parameter values are used that closely match both the viscosity and its temperature dependence in the vicinity of room temperature, the thermal diffusion factor at 300 K is found to lie within 0.04-0.06, which agrees with the experimental values. This agreement suggests that DSMC can be used to study thermal diffusion in gas mixtures with good accuracy if sufficiently accurate molecular models are available over the temperature range of interest.

The VSS model for carbon dioxide is accurate enough for quantitative predictions of thermal gas separation only when the temperature range is constrained to be rather small (e.g., not 300-600 K, but 275-325 K) and the VSS parameters are selected to match both the viscosity and its temperature dependence in this range. A more general molecular model is needed to represent carbon dioxide over a wide temperature range (e.g., 300-600 K, which corresponds to a nominal solar heat flux of 1 kW/m being conducted by air across a gap of 1 cm). To be useful, such a model would have to be compatible with the general architecture of the DSMC algorithm.

As discussed earlier, thermal gas separation has two aspects. The first aspect is the degree of static thermal separation that can be achieved, which is the focus herein. If molecular models for nitrogen and carbon dioxide are developed that are accurate over a wide temperature range, then thermal diffusion can be simulated accurately at both ambient and elevated temperatures, thereby providing the information needed for the second aspect. The second aspect involves enhancing thermal separation of carbon dioxide from air through vertical counter-flow from buoyant convection or through other flow-based approaches. To fully assess the feasibility of thermal separation of carbon dioxide from air, this second aspect must be investigated.

REFERENCES

Amdur et al., 1952: I. Amdur, J. W. Irvine, Jr., E. A. Mason, and J. Ross, "Diffusion Coefficients of the Systems CO_2–CO_2 and CO_2–N_2O," *Journal of Chemical Physics*, Vol. 20, No. 3, pp. 436-443, 1952.

Bartel et al., 2001: T. J. Bartel, S. J. Plimpton, and M. A. Gallis, *Icarus: A 2-D Direct Simulation Monte Carlo (DSMC) Code for Multi-Processor Computers*, User's Manual, Version 10.0, Sandia report SAND2001-2901, Sandia National Laboratories, Albuquerque, NM, 2001.

Bastick et al., 1939: R. E. Bastick, H. R. Heath, and T. L. Ibbs, "The Molecular Fields of Carbon Dioxide and Nitrous Oxide," *Proceedings of the Royal Society of London, Series A, Mathematical and Physical Sciences*, Vol. 173, No. 955, pp. 543-554, 1939.

Bird, 1994: G. A. Bird, *Molecular Gas Dynamics and the Direct Simulation of Gas Flows*, Clarendon Press, Oxford, UK, 1994.

Bird, Stewart, and Lightfoot, 1960: R. B. Bird, W. E. Stewart, and E. N. Lightfoot, *Transport Phenomena*, First Edition, John Wiley and Sons, New York, NY, 1960.

Bird, Stewart, and Lightfoot, 2007: R. B. Bird, W. E. Stewart, and E. N. Lightfoot, *Transport Phenomena*, Second Edition, John Wiley and Sons, New York, NY, 2007.

Chapman and Cowling, 1970: S. Chapman and T. G. Cowling, *The Mathematical Theory of Non-Uniform Gases*, Third Edition, Cambridge University Press, Cambridge, UK, 1970.

Clark Jones and Furry, 1946: R. Clark Jones and W. H. Furry, "The Separation of Isotopes by Thermal Diffusion," *Reviews of Modern Physics*, Vol. 18, No. 2, pp. 151-224, 1946.

Grew and Ibbs, 1952, K. E. Grew and T. L. Ibbs, *Thermal Diffusion in Gases*, Cambridge University Press, Cambridge, UK, 1952.

Hirschfelder, Curtiss, and Bird, 1954: J. O. Hirschfelder, C. F. Curtiss, and R. B. Bird, *Molecular Theory of Gases and Liquids*, John Wiley and Sons, New York, NY, 1954.

Lambert, 1977: J. D. Lambert, *Vibrational and Rotational Relaxation in Gases*, Clarendon Press, Oxford, UK, 1977.

White, 1984: F. M. White, *Heat Transfer*, Addison-Wesley Publishing Company, Reading, MA, 1984.

Winn, 1950: E. B. Winn, "The Temperature Dependence of the Self-Diffusion Coefficients of Argon, Neon, Nitrogen, Oxygen, Carbon Dioxide, and Methane," *Physical Review*, Vol. 80, No. 6, pp. 1024-1027, 1950.

DISTRIBUTION

1	MS 0346	C. F. Brooks	Org. 01513	
1	MS 0346	M. A. Gallis	Org. 01513	
1	MS 0346	D. J. Rader	Org. 01513	
4	MS 0346	J. R. Torczynski	Org. 01513	
1	MS 0384	A. C. Ratzel	Org. 01500	
1	MS 0824	J. S. Lash	Org. 01510	
1	MS 0734	C. L. Staiger	Org. 06338	
1	MS 0734	E. B. Stechel	Org. 06339	
1	MS 0754	P. V. Brady	Org. 06310	
1	MS 0776	C. R. Bryan	Org. 06786	
1	MS 0899	Technical Library	Org. 09536	(electronic copy)
1	MS 0123	D. L. Chavez, LDRD Office	Org. 01011	